V. Valdivia, R. Todd, F.J. Bryan, A. Barrado, A. Lazaro, A.J. Forsyth, "Behavioral Modeling of a Switched Reluctance Generator for Aircraft Power Systems," *IEEE Transactions on Industrial Electronics*, vol. 61, no. 6, pp. 2690-2699, June 2014, doi: 10.1109/TIE.2013.2276768

Behavioural Modelling of a Switched Reluctance Generator for Aircraft Power Systems

Virgilio Valdivia, *Student Member, IEEE*, Rebecca Todd, *Senior Member, IEEE*, Frank J. Bryan, Andrés Barrado *Senior Member, IEEE*, Antonio Lázaro, *Member, IEEE*, Andrew J. Forsyth, *Senior Member, IEEE*

***Abstract*—A system-level modelling technique for a switched reluctance generator (SRG) is described for aerospace applications. Unlike existing techniques, this model is very simple and only reproduces the average behaviour of the input-output variables that are required for system-level analysis of the aircraft power distribution system. The model is parameterised from the measured generator response, avoiding the need for a detailed knowledge of the equipment structure, which may be unavailable. The modelling procedure is described in detail and validated by measurements on a switched reluctance generator within an aircraft test facility.**

***Index Terms*— Switched Reluctance Generator, Aerospace, Modelling, System Identification**

I. Introduction

The more-electric-aircraft (MEA) concept is leading to an increase in on board electrical equipment to drive aircraft subsystems that have conventionally been supplied by pneumatic, hydraulic or mechanical means. The transition to MEA technologies is resulting in higher levels of on board electrical power, and more complex electrical subsystems [1]-[7]. Consequently there is a high risk of dynamic interactions and instability between the regulated power converters and motor drives within the system. Techniques are therefore required to allow these effects to be examined at the design stage, and to ensure good stability margins.

Manuscript received April, 2012; revised June, 2012, November 2012 and February 2013; accepted May, 2013.

During the development of this work, V. Valdivia was with the Carlos III University of Madrid, 28911 Leganes, Spain. He is now with United Technologies Research Center, Cork, Ireland (e-mail: guerrevv@utrc.utc.com).

A. Barrado and A. Lázaro are with the Carlos III University of Madrid, 28911 Leganes, Spain (e-mail: barrado@ing.uc3m.es, alazaro@ing.uc3m.es).

R. Todd, A. Forsyth and F. Bryan are with the Power Conversion Group, School of Electrical and Electronic Engineering, The University of Manchester, Manchester M13 9PL, U.K. e-mail: andrew.forsyth@manchester.ac.uk, rebecca.todd@manchester.ac.uk, frank.bryan@manchester.ac.uk

System-level dynamic models and simulations provide the basis to assure proper performance of a power distribution architecture [8]-[17]. Consequently, system-level behavioural models of power converters [18]-[26] have been recently developed as an alternative to conventional average-value or switched models. These models only compute the variables required for system level analysis (typically input-output signals), and can be parameterised from the measured converter response. Moreover, these models do not represent in detail the internal structure of the actual converter.

The switched reluctance machine (SRM) is one of the candidate technologies for future engine-embedded starter/generators due to its simple structure, robustness, and fault tolerance [27]-[31]. Existing modelling approaches for switched reluctance generators (SRGs) focus on a detailed description of the electromagnetic behaviour of the machine and switching behaviour of the converter [32]-[35]. As a result these models require a detailed knowledge of the internal structure of the machine and drive system. However, modern aerospace systems comprise many subsystems from a number of different manufacturers and the system designer may not have access to all internal details of each piece of equipment, which are required to build up a conventional SRG model. Also, excessively detailed models may lead to unacceptable simulation times when integrated together. Therefore these models are not well suited to system-level analysis.

To address these issues, a behavioural modelling technique for a SRG is proposed. The presented model is intended to be used for dynamic analysis of power distribution architectures at system-level, including stability, interactions with other subsystems, response during transients, etc [8]-[17]. The main features are:

- Simple representation of relationships between average terminal waveforms, leading to manageable system simulation times.
- Parameterization of dynamic components based on straightforward transient response measurements.
- The internal structure of the SRG is not represented in detail, thereby protecting confidential data.
- If required, the model can be provided with special features of the actual voltage controller, such as clamping or anti-windup functions.

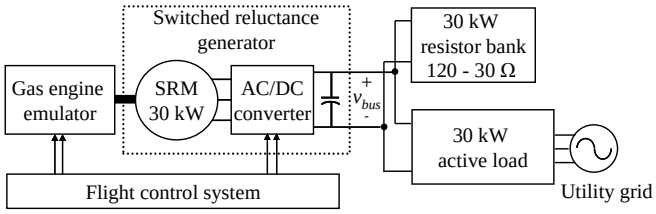

(a)

(b)

Fig. 1 Experimental system under study. a) Schematic b) Hardware

This paper is organised as follows:

- The system under study is described in Section II.
- The proposed model is presented in Section III.
- The parameterisation method is explained and applied to the experimental system under study in Section IV.
- The model is validated and demonstrated for system-level analysis in section V.

II. System Description

The sub-system under consideration in this work is shown in Fig 1 and comprises a commercial SRG which is driven by an engine emulator and loaded by a combination of resistive and active loads. The 30 kW SRG consists of a three-phase machine with twelve stator poles and eight rotor poles, and a conventional three-phase half-bridge converter. The SRG regulates the DC-bus at 540 V and supplies a maximum of 30 kW over a speed range of 7,000 rpm to 15,000 rpm.

The gas engine emulator is a 115 kW, 15,000 rpm, bidirectional induction machine drive and is commanded by the flight control system (FCS) which contains a generic two-spool gas engine model. The model takes environmental data, throttle position and electrical power off-take as inputs and outputs a speed command to the motor drive.

The active load can operate in constant current or constant power modes with a transient rise time of 10 ms. A detailed description of the aerospace system is given in [27].

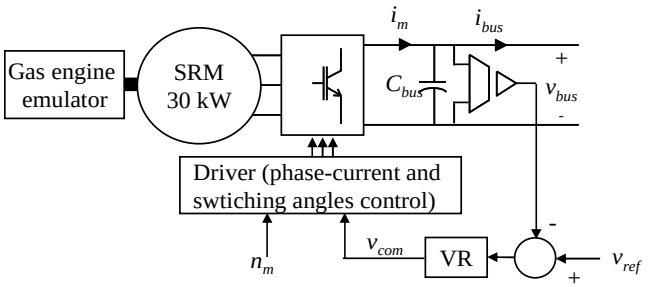

Fig. 2 Simplified schematic of SRG in generator mode

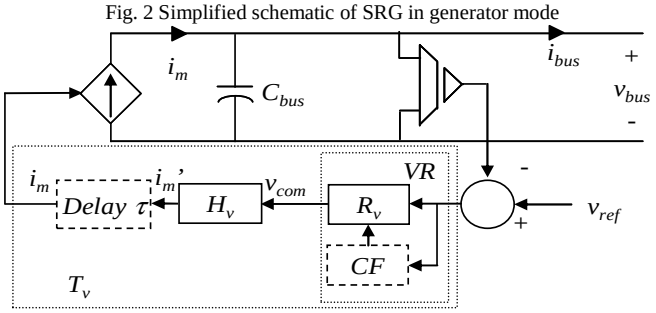

Fig. 3 Generator model

A block diagram of the SRG in generator mode is shown in Fig. 2. The error between the bus voltage v_{bus} and the reference signal v_{ref} passes through the voltage regulator *VR*, forming signal v_{com}, which, along with the machine speed n_m, commands the 'Driver' to set the power electronic switching pattern. Regulation schemes for switched reluctance generators are described in [35]-[37].

III. Modelling Approach

From a high level point of view the control stage may be considered to set the DC current, i_m, supplied by the SRG to the DC link capacitor and DC-bus to minimise the error between v_{ref} and v_{bus}. Therefore the power stage is modelled as a controlled current source feeding the DC-bus and capacitor C_{bus}, leading to the 'grey-box' behavioural model shown in Fig. 3, which partially represents the inner structure of the SRG.

The relationship between the error signal and the averaged SRM current, i_m, is represented by T_v which contains the elements of the actual controller, namely:

- Voltage regulator *VR*, comprising a linear proportional-integral term R_v, and any special functions such as clamping or anti-windup, denoted as "*CF*".
- H_v, which represents the dynamic relationship between the voltage regulator command, v_{com}, and the averaged machine current i_m, including the block 'Driver' and power stage.
- '*Delay* τ' accounts for any transport delay.

Mechanical speed transients are assumed to be relatively slow compared to the electrical transients so that they are not dynamically reflected in v_{bus}.

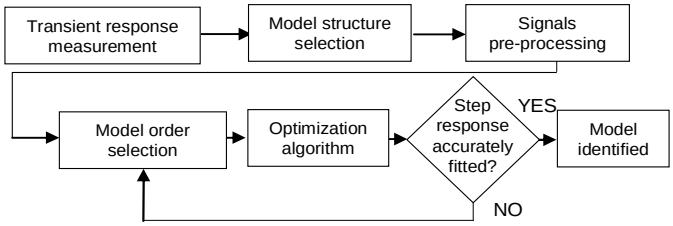

Fig. 4 Flowchart of the identification procedure of a transfer function model

The averaged dynamic relationship between v_{com} and i_m, modelled by H_v, may be in general dependent on operating point, due to the nonlinear characteristics of the SR machine. However, it was found that H_v exhibits only a slight non-linearity over the range of generator speed and power (shown in Section IV.E). Therefore H_v was assumed linear, providing a good compromise between model simplicity and performance. Nevertheless, dependence on operating point could be incorporated in the model by using a weighted combination of local linear models [22], [38].

Also, the 'grey-box' model structure allows retuning of the voltage control or alternative control topologies to be easily implemented by modifying *VR* in Fig. 3.

IV. Model Parameterisation

By applying a small-signal perturbation to i_{bus} in the model, Fig. 3, while v_{ref} is kept constant, the following expression for the output impedance is obtained:

$$-\left.\frac{v_{bus}(s)}{i_{bus}(s)}\right|_{v_{ref}(s)=0} = Z_o(s) = \frac{1}{\frac{1}{ZC_{bus}(s)} + T_v(s)} \tag{1}$$

where $T_v(s)$ is a linear representation of the block T_v in the Laplace domain (the *CF* block is disabled) and is given by (2). $e^{-\tau s}$ corresponds to the loop delay.

$$T_v(s) = R_v(s) H_v(s) e^{-\tau s} \tag{2}$$

As can be seen, $Z_o(s)$ corresponds to the parallel connection of the impedance of C_{bus}, $ZC_{bus}(s)$, with $T_v(s)^{-1}$. $Z_o(s)$ can therefore be used to obtain several parameters for the SRG model. The transfer function $Z_o(s)$ is identified in Section IV A. After that, C_{bus}, $T_v(s)$ and *CF* are characterized (Sections IV B, C and D, respectively).

A. Output impedance identification $Z_o(s)$

A transfer function model can be identified for $Z_o(s)$ from a set of input-output transient response measurements using parametric identification algorithms. These algorithms have been widely discussed in the literature [38], [39] and can be easily applied by using commercial tools, e.g. Matlab System Identification Toolbox [40]. A flowchart of the parametric identification procedure is depicted in Fig. 4 and described below.

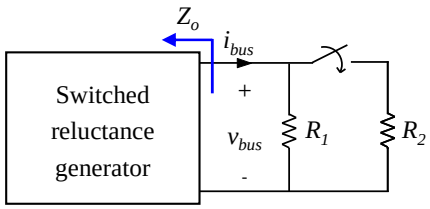

Fig. 5 Identification test of the output impedance Z_o of the SRG

1) Transient response measurements

A load step test is used to identify the output impedance, since it is easy to apply and leads to good identification results. The experimental setup comprises two resistors, R_1 and R_2, a switch and a data acquisition system, Fig. 5.

The step change should be small so that the system response can be assumed linear (the clamping and anti-windup functions, *CF* in Fig. 3, are not activated).

2) Model structure selection

The general transfer function model structure, identified through parametric methods, is:

$$y(k) = G(q)\cdot u(k) + H(q)\cdot e(k) \tag{3}$$

where $e(k)$ is white noise, $u(k)$ is the system input and $y(k)$ is the system output. $G(q)$ and $H(q)$ are the so-called input transfer function and error transfer function, respectively, and q is a shift operator ($q^{-1}x(k) = x(k-1)$). In this case $u(k)= i_{bus}(k)$, $y(k)= v_{bus}(k)$ and $G(q)= Z_o(q)$.

Depending on the characteristics of $G(q)$ and $H(q)$, several transfer function models are defined [38], [39]. In this work the Output Error (OE) model ($H(q)= 1$) is proposed, since a good trade-off between performance and complexity is achieved. This model structure has also been identified from step tests for system-level modelling of other converters in [23], [25], [26].

3) Signal pre-processing

Before identifying the model, the measured signals have to be pre-processed. First, their steady-state value has to be subtracted, since the transfer function model only accounts for the SRSG dynamics. Second, pre-filtering may be performed to minimise signal components which are not modelled by the transfer function (e.g. switching ripple). Both the input and the output signals have to be filtered using the same filter, otherwise the filter would be included in the identified model [38], [39].

4) Model order selection

Next, the model order of $G(q)$ has to be selected. Several choices should be iteratively tested until acceptable identification results are obtained. A good attempt can be done by looking at the waveform shape of the measured step response [24].

5) Optimisation algorithm

Following this, the optimisation algorithm is applied to obtain the coefficients of the transfer function model. An OE model can be identified using the "*oe*" function of Matlab, which searches for the coefficients of $G(q)$ by minimising the cost function COF given by (4). N is the number of samples.

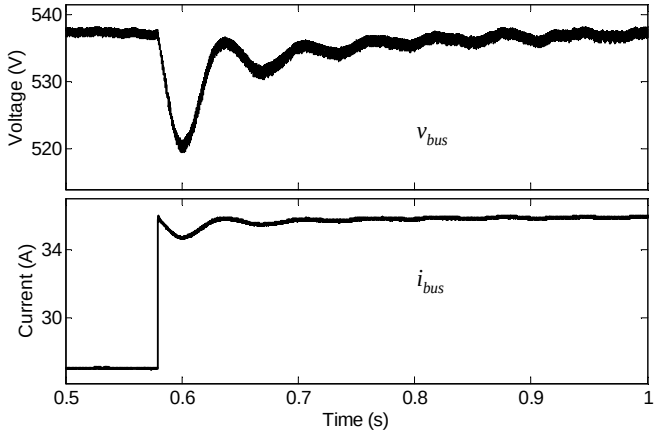

Fig. 6 SRG response under a load step from 15 kW to 20 kW at constant speed n_m = 7,000 rpm

$$COF = \sum_{k=1}^{N} \left(y(k) - G(q) \cdot u(k) \right)^2 \tag{4}$$

6) Validation of transfer function

The transfer function obtained from the optimisation algorithm is evaluated by comparing the model response with the measured response (after signal pre-processing). This can be done using the Matlab function "*compare*", which quantifies the fit as:

$$fit\% = 100 \cdot \left(1 - \frac{\sqrt{\sum_{k=1}^{N} \left(y(k) - \hat{y}(k) \right)^2}}{\sqrt{\sum_{k=1}^{N} \left(y(k) - \bar{y} \right)^2}} \right), \quad \bar{y} = \frac{1}{N} \sum_{k=1}^{N} y(k) \tag{5}$$

where $\hat{y}(k)$ is the model output, $\hat{y}(k) = G(q) \cdot u(q)$. If a poor fit is obtained then the model order should be adjusted.

Finally, the resulting discrete model can be converted to a continuous model by using a discrete to continuous time domain transformation, e.g. zero order hold or Tustin. More details about this procedure (Fig. 4) can be found in [25].

Experimental Identification

The procedure shown in Fig. 4 has been applied to the SRG. Fig. 6 illustrates the response of the SRG to a 5 kW resistive load step (no clamping functions are activated under this test, so linear behaviour is ensured).

Good identification results have been achieved with a third order model. Fig. 7 shows the identified transfer function response overlaid with the measured response (after signal preprocessing) and demonstrates a good correlation, a fit of 88.37 %.

The identified transfer function after transformation into the continuous domain is given by (6) and its frequency response is plotted in Fig. 8, where one can notice a low frequency pole at ≈1.6 Hz plus two complex conjugate poles at ≈14 Hz.

$$Z_o(s) = \frac{0.028s^3 + 140.6s^2 + 1.064 \cdot 10^4 s + 4782}{s^3 + 44.6s^2 + 8587s + 8.21 \cdot 10^4} \tag{6}$$

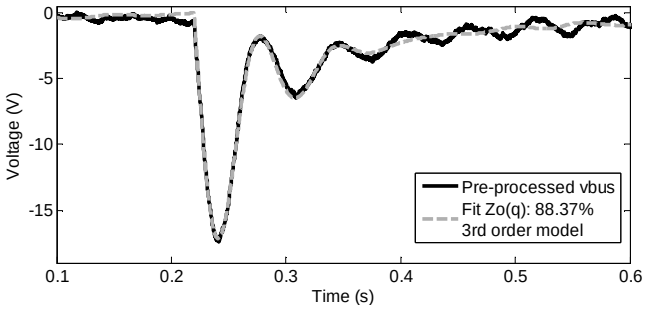

Fig. 7 Fitting results of $Z_o(q)$

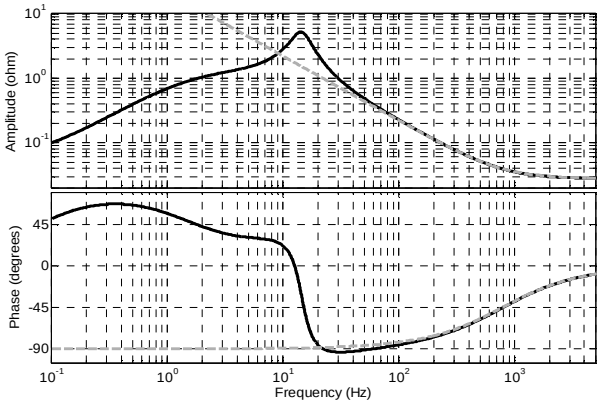

Fig. 8 Frequency response of the identified output impedance $Z_o(j\omega)$ (dark solid line) and the estimated output capacitor impedance $ZC_{bus}(j\omega)$ (grey dashed line)

B. Bus capacitor C_{bus}

According to (1), at high frequencies $Z_o(s) \approx ZC_{bus}(s)$ so, by analyzing $Z_o(j\omega)$ at high frequencies (where $Z_o(j\omega)$ exhibits capacitive behaviour) $ZC_{bus}(s)$ can be identified. In this case, $Z_o(j\omega)$ exhibit capacitive behaviour above 50 Hz, and $ZC_{bus}(s)$ can be approximated by a capacitance of 7.2 mF from Fig. 8.

Concerning the equivalent series resistance (ESR), 28 mΩ was estimated. Nevertheless, an accurate estimation of the ESR of 540 V capacitors from the step response is difficult, as its value is relatively small. Alternatively, the bus capacitor could be estimated from direct measurements at the output port using an impedance meter or impedance analyzer, as long as it is externally accessible.

C. Regulation and machine dynamics T_v

Once $ZC_{bus}(s)$ has been identified, $T_v(s)$ can be obtained as

$$T_v(s) = Z_o(s)^{-1} - ZC_{bus}(s)^{-1} \tag{7}$$

However, using (7) yields an unstable transfer function if a non-minimum phase transfer function is identified for $Z_o(s)$. Such a problem can be overcome by considering that according to Fig. 3, under linear operation $T_v(s)$ is dynamically related to the average machine current $i_m(s)$ as

$$T_v(s) = -\left. \frac{i_m(s)}{v_{bus}(s)} \right|_{v_{ref}(s)=0} \tag{8}$$

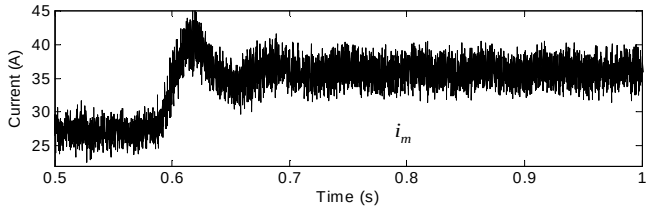

Fig. 9 Estimated machine current i_m

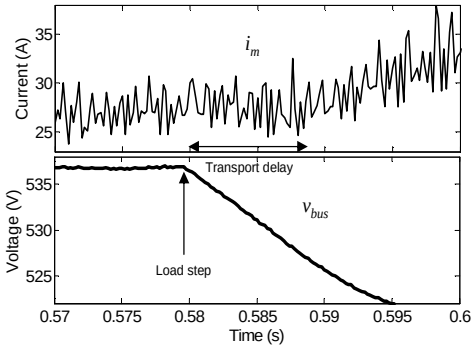

Fig. 10 Transport delay between the load switching and the beginning of the i_m transient response

Thus, if i_m is estimated from the measurements as:

$$i_m(k) = ZC_{bus}(q)^{-1} \cdot v_{bus}(k) + i_{bus}(k) \tag{9}$$

$T_v(s)$ can be identified from i_m and v_{bus} by applying parametric identification.

The estimated machine current, i_m, calculated from (9) and the waveforms depicted in Fig. 6 (v_{bus} and i_{bus}), is shown in Fig. 9. It exhibits a large amount of high frequency ripple due to the large magnitude of $ZC_{bus}(q)^{-1}$ at high frequency.

A transport delay of approximately 8 ms is apparent between the load step and the beginning of the transient response of i_m as shown in Fig. 10.

Hence, if $T_v(s)$ is identified directly from i_m and v_{bus}, then the transfer function model will include the delay. An alternative approach is to shift the estimated machine current i_m as in (10).

$$i_m'(k) = i_m(k + \tau \cdot f_s) \tag{10}$$

where i_m' is the shifted current, τ the transport delay and f_s the sampling frequency. This allows the transfer function model, (11), corresponding to the product of $R_v(s)H_v(s)$ to be identified from i_m' and v_{bus}.

$$R_v(s)H_v(s) = -\left.\frac{i_m'(s)}{v_{bus}(s)}\right|_{v_{ref}(s)=0} \tag{11}$$

Therefore $T_v(s)$ has been characterized as follows:

- i_m has been shifted 8 ms with respect to v_{bus} as given by (10). Then the delay in the model has been characterized as τ = 8ms.
- A transfer function model, corresponding to $R_v(s)H_v(s)$ has been identified from i_m' and v_{bus}.

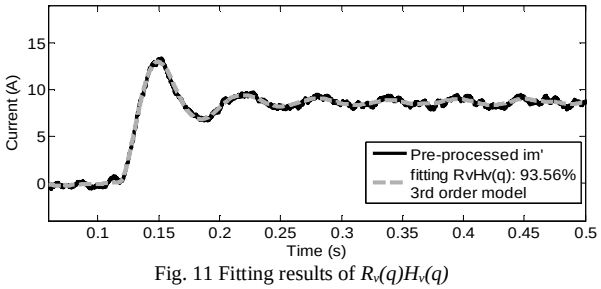

Fig. 11 Fitting results of $R_v(q)H_v(q)$

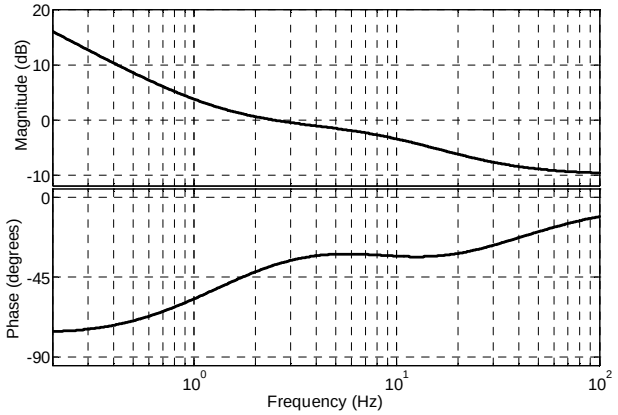

Fig. 12 Frequency response of $R_v(j\omega)H_v(j\omega)$

The identification of the transfer function model has been carried out by following the procedure shown in Fig. 4 but in this case $y(k) = i_m'(k)$, $u(k) = v_{bus}(k)$ and $G(q) = R_v(q)H_v(q)$. Both i_m' and v_{bus} have been pre-filtered using a moving average filter of 25 samples (f_s = 5 kHz) to attenuate the high frequency ripple.

The results are depicted in Fig. 11, where it is shown that the average behaviour of i_m' (after pre-filtering and offset subtraction) is accurately fitted by a third order transfer function.

The resulting transfer function after transformation into the continuous time domain is given by (12) and its frequency response is shown in Fig. 12, where some properties of the regulator, such as the low-frequency integrator, are apparent.

$$R_v(s)H_v(s) = \frac{0.2933s^3 + 2987s^2 + 5.38 \cdot 10^5 s + 4.622 \cdot 10^6}{s^3 + 9288s^2 + 5.81 \cdot 10^5 s + 9.176 \cdot 10^4} \tag{12}$$

Once $R_v(s)H_v(s)$, C_{bus} and τ have been characterized, the fitting performance of the overall generator model has been evaluated by comparing the frequency response of the identified output impedance $Z_o(s)$ (6) with that of the resulting model (1). As shown in Fig. 13, the output impedance of the model is very close to that directly identified from the measured load step, so the model has been correctly parameterised.

Any prior knowledge about parameters such as the bus capacitor C_{bus} or the regulator tuning / architecture can be readily used to parameterise the model, simplifying the procedure.

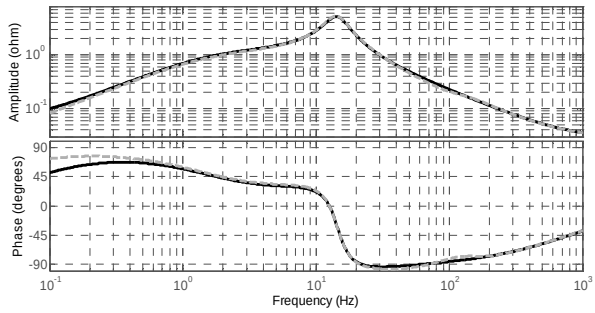

Fig. 13 Comparison between the output impedance of the SRG model (grey dashed line) with the output impedance of the actual converter (black solid line), directly identified from the measured v_{bus} and i_{bus} and shown in Fig. 8.

D. Clamping functions CF

Sometimes the voltage regulator may contain special features, such as clamping or anti-windup functions, which are activated under certain situations and may influence the dynamic response of the SRG significantly. The proposed 'grey-box' model allows the implementation of this kind of function, denoted as *CF* in Fig. 3.

A formal methodology to incorporate clamping functions in the voltage controller is difficult to define. In this case a heuristic technique was employed based on fragmented intelligence from the designer and manufacturer together with experimental step response tests over the full operating range of the system. The relation between the clamping function parameters and experimental data is shown later in Fig. 16. A number of iterations were necessary to refine the modelling of the clamping functions and improve the fitting between the simulation and experimental results, ensuring an accurate controller representation over all operating conditions.

The clamping functions of the SRG under experimental study act as follows on the voltage compensator, which is a *PI* type.

- The output of the proportional term K_p is clamped to zero while v_{ref} - v_{bus} < 0 V.
- The output of the integral term K_i is reset if v_{ref} - v_{bus} < - 18 V.
- The minimum value of the regulator output, v_{com}, is limited to zero if the commanded signal from the *PI* is lower than zero.

These clamping functions are activated during a step down in load to limit the maximum output voltage of the generator.

Fig. 14 illustrates the behaviour of the clamping functions under a load step from 20 kW to 15 kW at n_m = 7,000 rpm. When the load is reduced, v_{bus} increases because the difference between i_m and i_o charges C_{bus}. Consequently, the proportional term is disabled. Once v_{ref} - v_{bus} < -18 V, the integral term is reset, v_{com} = 0 and then v_{bus} decreases suddenly. Finally, when v_{ref} - v_{bus} ≥ 0 V the regulator is re-enabled to control v_{bus}.

To implement the clamping features of the voltage regulator, *VR*, the identified transfer function $R_v(s)H_v(s)$ has been split in two. By expressing (12) in a zero-pole-gain representation, the following expression is obtained:

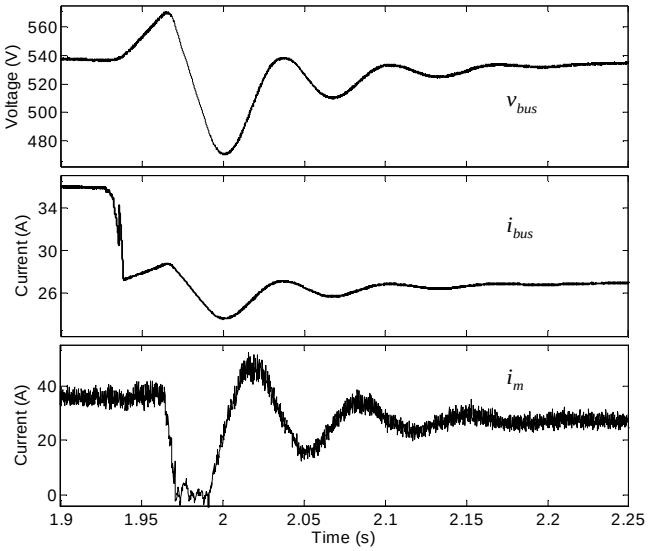

Fig. 14 SRG response under a load step from 20 kW to 15 kW at constant speed n_m = 7,000 rpm

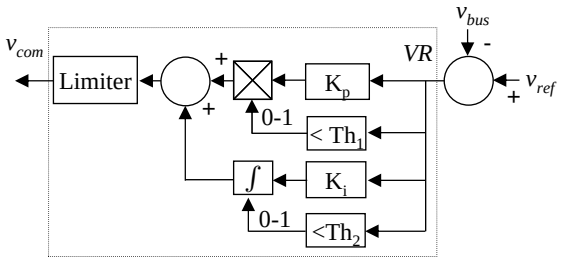

Fig. 15 Implementation of the *VR* block with clamping functions *CF*

$$R_v(s)H_v(s) = 0.293 \cdot \frac{(s+9.04)(s+174.2)(s+10000)}{(s+0.158)(s+62.8)(s+9226)} \qquad (13)$$

where the dominant, lowest frequency pole-zero pair corresponds to the *PI* compensator $R_v(s)$. By moving the lowest frequency pole to s→0 and neglecting the high frequency pole-zero pair, expressions for $R_v(s)$ and $H_v(s)$ are obtained as:

$$R_v(s) = \frac{s+9.04}{s} \qquad H_v(s) = 0.31 \cdot \frac{s+174.2}{s+62.82} \qquad (14)$$

From $R_v(s)$ the proportional and integral terms of the *PI* regulator are obtained: K_p = 1 and K_i = 9.04.

Moreover, when v_{com} = 0, it has been found that the SRM is rapidly de-energized so that i_m suddenly decreases to zero with a slew rate of 4.2 A/ms (Fig. 14). This nonlinear effect cannot be accounted for by the transfer function model $H_v(s)$. In order to reproduce such an effect, $H_v(s)$ has been represented in a state-space form with a resettable integrator followed by a slew-rate limiter. This integrator is reset when v_{com} = 0 and then the machine de-energizing is properly reproduced.

The resulting implementation of the *VR* block presented in Fig. 3, including the clamping functions *CF*, is shown in Fig. 15, where Th_1 = 0 and Th_2 = -18.

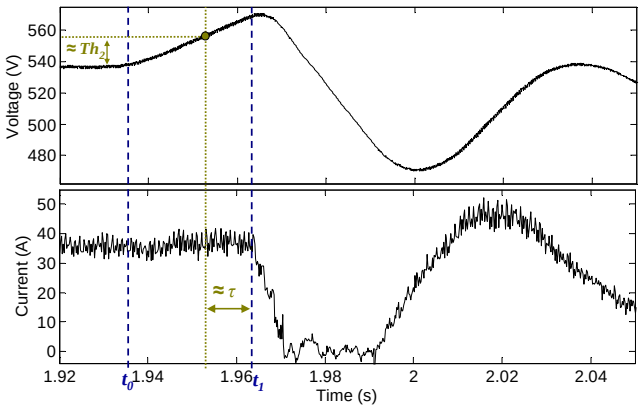

Fig. 16 Expanded view of Fig. 14 to demonstrate the process for estimating the parameters of the clamping function

Fig. 16 is an expanded view of bus voltage and machine current from Fig. 14; power is reduced from 20 kW to 15 kW at time t_0, shown in Fig. 16.

The clamping function parameters in Fig. 15 can be identified from this data through the following steps:

- At time t_0 the load step occurs. The current i_m responds approximately 26 ms after t_0, which is significantly slower than the 8 ms transport delay identified in Fig. 10 for a step up in load. This indicates that K_p, has been disabled as soon as v_{ref} - v_{bus} < 0, making the controller significantly slower. Therefore, the threshold Th_1 in Fig. 15 is estimated at zero.
- At time t_1, the machine current rapidly decreases, indicating that K_i has been disabled, so that v_{com} = 0. If the transport delay τ (8 ms from Fig. 10) is subtracted from t_1 then the threshold Th_2 can be estimated from the voltage difference in Fig. 16 as -18V.
- The v_{com} saturation limit of zero can also be deduced from Fig. 16, as i_m is always a positive value.

The clamping functions are specific to the SRG under test, but allows the flexibility of the proposed 'grey-box' behavioural model to be demonstrated, as special features such as clamping functions, anti-windup or other features of the actual controller can easily be included in the model.

The SRG behavioural model presented in Section IV is capable of regeneration (power flowing from the DC bus into the SRG) up to full current if minor modifications are made to the controller. The modifications to the controller, Fig. 15, are:

1. The K_p component is enabled for negative deviations in DC bus voltage (the reset on the K_p term is disabled). Without this v_{com} and the DC current of the SRM would be zero and there would be no power flow.
2. The zero limit on the v_{com} signal is disabled to allow v_{com} to be negative for regeneration

An additional modification to the controller is required to prevent overvoltage conditions; the reset on the K_i component is disabled, otherwise this would limit the functionality of the integral component and cause poor regulation of the DC voltage.

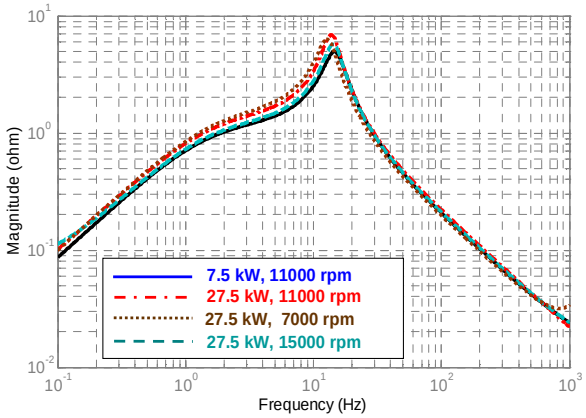

Fig. 17 Analysis of output impedance dependence on operating point: given by power level and speed.

E. *Justification for linearity assumption*

Fig. 17 shows the frequency response of the output impedance identified by applying 5 kW steps for different load and speed conditions (the clamping function is disabled). The power listed in the figure is the intermediate power level.

In Fig. 17 the generator exhibits a resonant frequency at approximately 14 Hz for all operating conditions shown with all responses being very similar above the resonant frequency, as the response in dominated by C_{bus}. Below the resonant frequency there is a slight dependence on operating condition. This dependence has been neglected to simplify the model and so H_v is represented as a LTI system.

V. Model Validation

The 'grey-box' model of the SRG has been implemented in the circuit simulator PSIM for validation purposes. A set of load step tests have been carried out both experimentally and by simulation, and the results from both tests have been compared. Both a passive and a constant power load have been used.

1) Passive load steps

Several resistive load steps with different magnitudes have been performed at different speeds in order to validate the model behaviour over the full operating range, as shown in Fig. 18.

Fig. 19 shows a comparison between the measured response and the simulated response for two 5 kW load steps. The first test, shown in Fig. 19.a, corresponds to that used for model identification (15 kW to 20 kW at n_m = 7,000 rpm). As may be expected, the model response is very close to the measured response.

The second test, shown in Fig. 19.b, is a step from 25 kW to full load (30 kW) at n_m = 11,000 rpm. Small differences between the model response and the measured response are observed. Those differences are due to slight nonlinearities of the SRM not reproduced by the model, since the block H_v has been approximated by a LTI model.

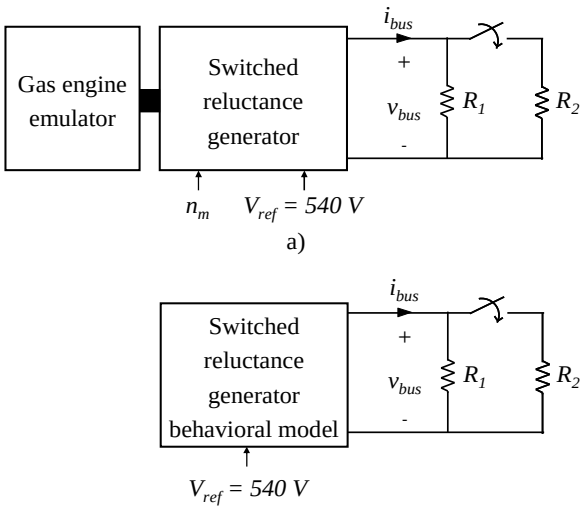

Fig. 18 Validation of the model under generating operation with a passive stepped load a) Experimental setup b) Simulated schematic

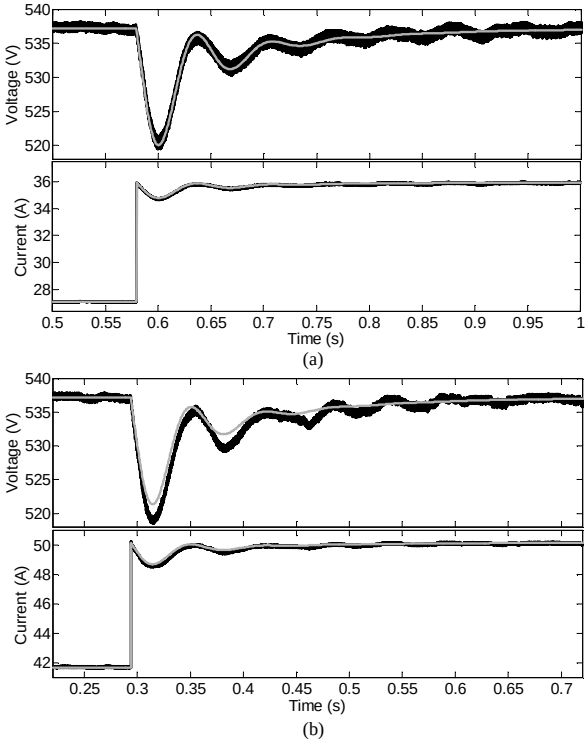

Fig. 19 Measured response (black traces) vs simulated response (grey traces) under resistive load steps a) from 15 kW to 20 kW at n_m = 7,000 rpm. b) from 25 kW to 30 kW at n_m = 11,000 rpm

Fig. 20 shows validation results for a step increase and decrease in load from 10 kW to 20 kW and back at maximum speed, 15,000 rpm. The non-symmetrical behavior of the SRG is evident and is due to the activation of the clamping functions during the step decrease in load. As can be seen, the model reproduces properly the response of the SRG both under increases and decreases in load. This validates the clamping functions implemented in the model.

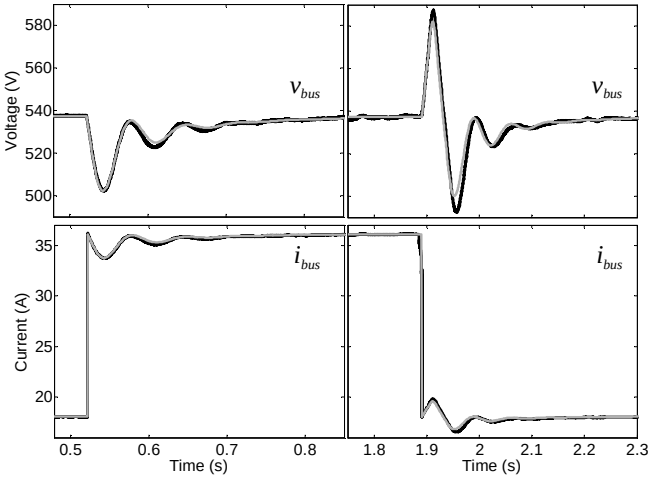

Fig. 20 Measured response (black traces) vs simulated response (grey traces). Resistive load step up from 10 kW to 20 kW followed by a step down to 10 kW at n_m = 15,000 rpm

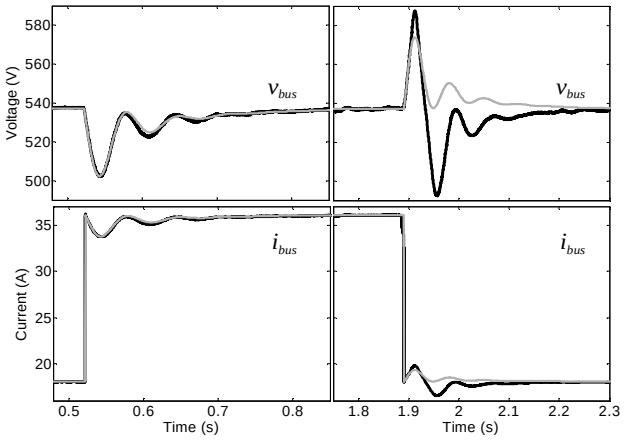

Fig. 21 Measured response (black traces) vs simulated response (grey traces). Resistive load step up from 10 kW to 20 kW followed by a step down to 10 kW at n_m = 15,000 rpm without the clamping functions *CF* in the simulation model

To illustrate the importance of the clamping functions, the simulation result in Fig. 20 has been repeated with the *CF* block disabled. The results (Fig. 21) are unchanged in response to the load increase but there are significant discrepancies when the load is reduced, particularly in terms of the peak deviation of the voltage.

2) Constant power load steps

With the active load configured in constant power mode, the generator system was subjected to load step changes as in Fig. 22.a. The load is commanded by a high bandwidth control loop (around 3 kHz) so, for the purpose of simulation, it was assumed to be infinite. Hence, the active load has been simulated in PSIM as shown in Fig. 22.b, where the input filter capacitor is 110 μF.

The measured and simulated responses for step increases and decreases in power load are shown in Fig. 23.a and Fig. 23.b. The simulated response is close to the measured one in all cases. The observed differences are relatively small and, as

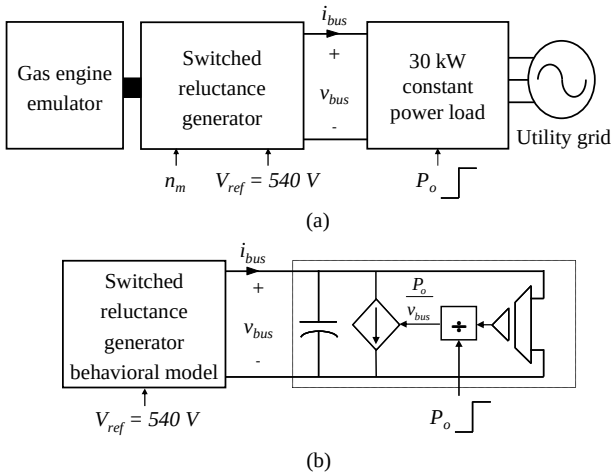

Fig. 22 Validation of the model under generating operation and constant power load steps a) Experimental setup b) Simulated schematic

discussed earlier, they are due to slight nonlinearities of the SRM which are not accounted for by the model. Nevertheless, the key transient response characteristics such as the settling time and the overshoot are predicted by the model with a good degree of accuracy.

VI. Conclusions

A behavioural modelling technique for a switched reluctance generator is proposed. The model is simple, reproduces the average behaviour of the input-output signals of the generator and can be fully parameterised using a set of simple tests. The model is particularly suitable for system level studies such as examining power generation and distribution on board a more-electric aircraft.

A comprehensive illustration of the proposed methodology has been presented by making use of a switched reluctance generator located in an aerospace test facility. For validation purposes, the model has been implemented in a virtual test bench and its response has been compared to that of the real system under a variety of tests over the whole operating range of the generator, consisting of passive and active load steps. In all cases, the model has reproduced with good accuracy the actual system response. The capability of the model to include nonlinear functions of the regulator, such as clamping or anti-windup, has also been illustrated.

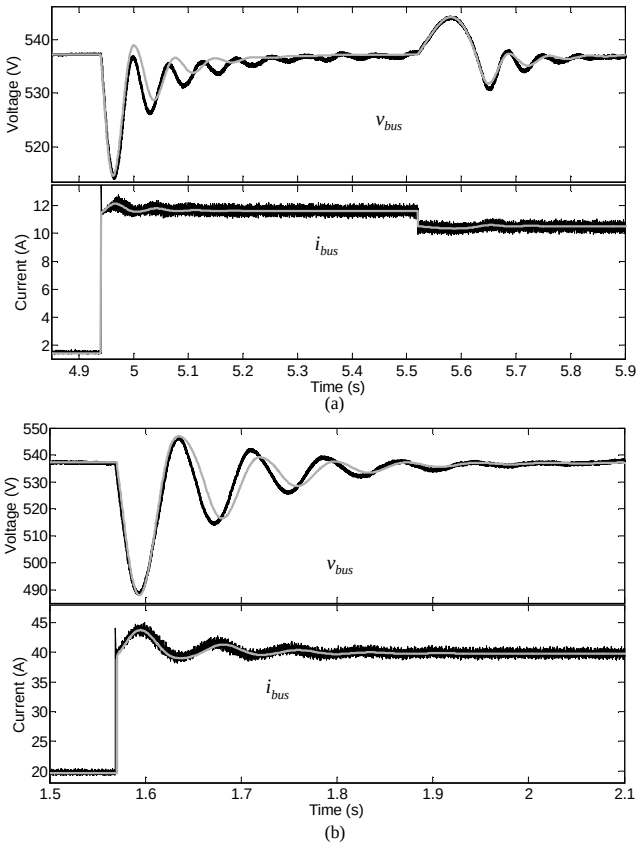

Fig. 23 Measured response (black traces) vs simulated response (grey traces) under constant power load steps at n_m = 7,000 rpm. a) Step from 850 W to 6.3 kW followed by a step down to 5.6 kW b) Step from 11 kW to 22 kW

References

[1] W. Cao, B. Mecrow, G. Atkinson, J. Bennett, D. Atkinson, "Overview of Electric Motor Technologies Used for More Electric Aircraft (MEA)" *IEEE Trans. Ind. Electron., vol. 59, no. 9, pp. 3523 – 3531, 2012.*

[2] D. Izquierdo, R. Azcona, F. del Cerro, C. Fernandez, B. Delicado, "Electrical Power Distribution System (HV270DC), for Application in More Electric Aircraft", *in Proc. of IEEE Appl. Power Electron. Conf. (APEC), pp 1300 - 1305, 2010.*

[3] H. Zhang, F. Mollet, C. Saudemont, B. Robyns, "Experimental Validation of Energy Storage System Management Strategies for a Local DC Distribution System of More Electric Aircraft", *IEEE Trans. Ind. Electron., vol. 57, no. 12, pp. 3905 – 3916, 2010.*

[4] J. Bennett, G. Atkinson, B. Mecrow, D. Atkinson, "Fault Tolerant Design Considerations and Control Strategies for Aerospace Drives", *IEEE Trans. Ind. Electron., vol. 59, no. 5, pp. 2049 – 2058, 2012.*

[5] A. Griffo, D. Drury, T. Sawata, P.H. Mellor, "Sensorless Starting of a Wound-Field Synchronous Starter/Generator for Aerospace Applications", *IEEE Trans. Ind. Electron., vol. 59, no. 9, pp. 3579 – 3587, 2012.*

[6] D. Izquierdo, A. Barrado, C. Fernandez, M. Sanz, A. Lazaro, "SSPC Active Control Strategy by optimal trajectory of the current for onboard systems applications", *IEEE Trans. Ind. Electron., forthcoming papers, DOI 10.1109/TIE.2012.2219832*

[7] D. Izquierdo, A. Barrado, C. Raga, M. Sanz, A. Lazaro, "Protection Devices for Aircraft Electrical Power Distribution Systems: State of the Art", *IEEE Trans. Aero. Electron. Sys., vol. 47, no. 3, pp. 1538 – 1550, 2011.*

[8] L. Han, J. Wang, D. Howe, "Stability Assessment of Distributed DC Power Systems for 'MoreElectric' Aircraft", *in Proc. of the 4th IET International Conference on Power Electronics, Machines and Drives, pp. 162 – 166, 2008.*

[9] R. Burgos, S. Rosado, F. Wang, D. Boroyevch, Z. Lewis and K. Karimi, "Modeling Considerations and Stability Analysis of Aerospace Power Systems with Hybrid AC/DC Distribution," *SAE Pow. Sys. Conf, 2006.*

[10] I. Cvetkovic, D. Boroyevich, P. Mattavelli, F. C. Lee, D. Dong, "Non-linear, Hybrid Terminal Behavioral Modeling of a DC-based Nanogrid System," *in Proc. of IEEE Appl. Power Electron. Conf. (APEC), pp. 1251 - 1258, 2011.*

[11] P. Magne, B. Nahid-Mobarakeh, S. Pierfederici, "General Active Global Stabilization of Multiloads DC-Power Networks," *IEEE Trans. on Power Electron.*, vol. 27, no. 4, pp.1788-1798, 2012

[12] Bozhko, S.V.; Wu, T.; Asher, G.M.; Wheeler, P.W., "Accelerated functional-level modeling of more-electric aircraft electrical power

system", *in proc. Of Electrical Systems for Aircraft, Railway and Ship Propulsion (ESARS), 2010, pp. 1-6.*

[13] P. Magne, B. Nahid-Mobarakeh, S. Pierfederici, "Active Stabilization of DC Microgrids without Remote Sensors for More Electric Aircrafts," *IEEE Trans. on Ind. Appl., early version*, DOI:10.1109/TIA.2013.2262031, 2013

[14] K. Areerak, T. Wu, S.V. Bozhko, G.M. Asher, D.W.P. Thomas, "Aircraft Power System Stability Study Including Effect of Voltage Control and Actuators Dynamic," *IEEE Trans. Aero. Electron. Sys.*, vol. 47, no. 4, pp. 2574-2589, 2011

[15] Areerak, K.; Bozhko, S.V.; Asher, G.M.; De Lillo, L.; Thomas, D.W.P. , "Stability Study for a Hybrid AC-DC More-Electric Aircraft Power System", *IEEE Trans. Aero. Electron. Sys.*, vol. 48, no. 1, 2012 , Page(s): 329 - 347.

[16] Griffo, A.; Jiabin Wang, "Large Signal Stability Analysis of 'More Electric' Aircraft Power Systems with Constant Power Loads", *IEEE Trans. Aero. Electron. Systems*, vol. 48, no. 1, 2012 , pp. 477 - 489.

[17] S. Vesti, P. Alou, J.A. Oliver, O. Garcia, R. Prieto, J.A. Cobos, "Modeling and Simulation of a Distributed Power System for Avionic Application", *in Proc. of IEEE Energy Conversion Congress and Exposition (ECCE), pp. 4421 – 4427, 2010.*

[18] J. Oliver, R. Prieto, J. Cobos, P. Alou, O. Garcia, "Hybrid Wiener-Hammerstein Structure for Grey-Box Modeling of DC DC Converters," *in Proc. of IEEE Appl. Power Electron. Conf. (APEC), pp. 280 - 285, 2009.*

[19] L. Arnedo, R. Burgos, D. Boroyevich, F. Wang, "System-Level Black-Box Dc to Dc Converter models", *in Proc. of IEEE Appl. Power Electron. Conf. (APEC), pp. 1476 – 1481, 2009.*

[20] I. Cvetkovic, M. Jaksic, D. Boroyevich, P. Mattavelli, F.C. Lee, Zhiyu Shen; S. Ahmed, Dong Dong, "Un-Terminated, Low-Frequency Terminal-Behavioral d-q Model of Three-Phase Converters", *in Proc. of IEEE Energy Conversion Congress and Exposition (ECCE), pp. 791 - 798, 2011.*

[21] Cvetkovic, I. ; Boroyevich, D. ; Mattavelli, P. ; Lee, F. C. ; Dong, D. "Unterminated Small-Signal Behavioral Model of DC–DC Converters", *IEEE Trans. Power Electron.*, vol. 28, no. 4, 2013 , pp. 1870-1879

[22] L. Arnedo, D. Boroyevich, R. Burgos, F. Wang, "Polytopic Black-Box modeling of DC-DC converters", *in Proc. of IEEE Power Electron. Specialists Conf. (PESC), pp. 1015 - 1021, 2008.*

[23] V. Valdivia, A. Barrado, A. Lazaro, C. Fernandez, P. Zumel, "Black-Box Modeling of DC-DC Converters Based on Transient Response Analysis and Parametric Identification Methods", *in Proc. of IEEE Appl. Power Electron. Conf. (APEC), pp. 1131 – 1138, 2010.*

[24] V. Valdivia , A. Barrado , A. Lazaro , P. Zumel, C. Raga, C. Fernandez "Simple Modeling and Identification Procedures for 'Black-Box' Behavioral Modeling of Power Converters Based on Transient Response Analysis", *IEEE Trans. Power Electron., vol. 24, no. 12, pp. 2776 - 2790, 2009.*

[25] V. Valdivia, A. Lazaro, A. Barrado, P. Zumel, C. Fernandez, M. Sanz, "Black-Box Modeling of Three Phase Voltage Source Inverters for System-Level Analysis" *IEEE Trans. Ind. Electron., vol. 59, no. 9, pp. 3648 - 3662, 2012.*

[26] V. Valdivia, A. Barrado, A. Lazaro, M. Sanz, D. Lopez del Moral, C. Raga, "Black-Box Behavioral Modeling and Identification of DC-DC Converters with Input Current Control for Fuel Cell Power Conditioning", *IEEE Trans. Ind. Electron, early version, 2013*, 10.1109/TIE.2013.2267692

[27] R. Todd, A.J Forsyth. "HIL Emulation of All-Electric UAV Power Systems", *in Proc. of IEEE Energy Conversion Congress and Exposition (ECCE), pp. 411 – 416, 2009.*

[28] C. A. Ferreira, S. R. Jones, W. S. Heglund, W. D. Jones, "Detailed Design of a 30-kW Switched Reluctance Starter/Generator System for a Gas Turbine Engine Application", *IEEE Trans. Ind. Applicat., vol. 31, pp. 553 - 561 , 1995.*

[29] A. V. Radun, C. A. Ferreira, E. Richter, "Two Channel Switched Reluctance Starter/Generator Results," *IEEE Trans. Ind. Appl., vol. 34, no. 5, pp. 1026 – 1034, 1998.*

[30] N. Schofield, S. Long, "Generator Operation of a Switched Reluctance Starter/Generator at Extended Speeds", *IEEE Trans. on Vehicular Technology, vol. 58, no. 1, pp. 48 – 56, 2009.*

[31] Z. Chen, H. Wang, Y. Yan, "A Doubly Salient Starter-Generator with Two-Section Twisted-Rotor Structure for Potential Future Aerospace Application", *IEEE Trans. Ind. Electron., vol. 59, no. 9, pp. 3588 – 3595, 2012.*

[32] O. Ichinokura, T. Kikuchi, K. Nakamura, T. Watanabe, H. Guol, "Dynamic Simulation Model of Switched Reluctance Generator," *IEEE Trans. Mag., vol. 39, no.5, part 2, pp. 3253 - 3255, 2003.*

[33] C. Zhuping, L. Deliang, "Simulation of Switched Reluctance Starter/Generator System Based on Simplorer", *in Proc. of the 8th Int. Conf. on Electrical Machines and Systems (ICEMS), vol. 1, pp. 564 - 567, 2005.*

[34] W. Ding, D. Liang, "A Fast Analytical Model for an Integrated Switched Reluctance Starter/Generator", *IEEE. Trans. Energy Conv. vol. 25, no. 4, pp. 948 - 956, 2010.*

[35] D. B. Wicklund, D. S. Zinger, "Voltage Feedback Signal Conditioning in Switched Reluctance Generation Systems", *Proc. IEEE Appl. Power Electron. Conf. Expo (APEC), pp. 376 - 380, 2000.*

[36] D. A. Torrey, "Switched Reluctance Generators and their Control", *IEEE Trans. Ind. Electron., vol. 49, no. 1, pp. 3 - 14, 2002.*

[37] Y. Chang, C. Liaw, "On the Design of Power Circuit and Control Scheme for Switched Reluctance Generator", *IEEE Trans. Power Electron., vol. 23, no. 1, pp. 445 - 454, 2008.*

[38] O. Nelles "Nonlinear System Identification, 1st ed.", *Springer-Verlag, 2000.*

[39] L. Ljung, "System Identification: Theory for the user, 2nd ed.", *Prentice Hall, 1999.*

[40] L. Ljung, "System Identification Toolbox 7", User's Guide, The Mathworks Inc. Natick, MA, 2007.

Virgilio Valdivia (S'07) was born in Barcelona, Spain, in 1983. He received the M.Sc. and Ph.D. degree in electrical engineering from Carlos III University of Madrid, Leganés, Spain, in 2006 and 2013, respectively. From October 2006 to September 2012, he was with the Carlos III University of Madrid as a Research Engineer. Since September 2012, he has been with United Technologies Research Center, Cork, Ireland, as a senior Research Engineer. He has also been a visiting researcher at the European Space Research and Technology Centre in 2009, the Rolls Royce University Technology Centre at the University of Manchester in 2011, and the Center for Power Electronics Systems at Virgina Tech in 2012.

His research interest includes modeling, identification and control of power electronics converters, energy microgrids and aerospace systems.

Rebecca Todd (M'08-SM'12) received the M.Eng. degree from the University of Manchester Institute of Science and Technology, Manchester, U.K., in 2001 and the Eng.D. degree from the University of Manchester, Manchester, U.K., in 2006.

She was a Research Associate in the Rolls-Royce University Technology Centre from 2006 to 2010, and since 2010 has been a Lecturer at The University of Manchester. Her research interests include advanced control methods, supercapacitor-based energy storage devices and energy management for on-board electrical systems comprising multiple, engine embedded generators and power electronic motor drive loads.

Frank Bryan was born in Liverpool, UK in 1983. He received the M.Eng. degree in Mechatronics from UMIST, Manchester, U.K., in 2006 and the Eng.D. degree in 2011 from The University of Manchester, U.K.

He has since held the post of Research Associate at The Rolls-Royce University Technology Centre at The University of Manchester. His research interests include power dense converters for aerospace and automotive applications.

Andrés Barrado (M'00-SM'11) was born in Badajoz, Spain, in 1968. He received the M. Sc. degree in electrical engineering from Polytechnic University of Madrid, Spain, in 1994, and the Ph.D. degree from Carlos III University of Madrid, Spain, in 2000. He is Professor at Carlos III University of Madrid, and since 2004 Head of the Power Electronics Systems Group (GSEP). His research interests are: switching-mode power supply, inverters, power factor correction, solar and fuel cell conditioning, behavioural modelling of converters and systems, fuel cell electric vehicle (FCEV) and power distribution systems for aircrafts. He has published over 150 scientific papers in international journals and conference proceedings and holds 11 patents. He has been actively involved in over 65 R&D projects for companies in Europe and the U.S.

Dr. Barrado is a member of the IEEE-PELS-IES Spanish Chapter.

Antonio Lázaro (M'97) was born in Madrid, Spain, in 1968. He received the M. Sc. in electrical engineering from the Universidad Politécnica de Madrid, Spain, in 1995. He received the Ph. D. in Electrical Engineering from the Universidad Carlos III de Madrid in 2003.

He has been an Assistant Professor of the Universidad Carlos III de Madrid since 1995. He has been involved in power electronics since 1994, participating in more than 50 research and development projects for industry. He holds seven patents and software registrations and he has published nearly 125 papers in IEEE journals & conferences. His research interests are switched-mode power supplies, power factor correction circuits, inverters (ups and grid connected applications), modeling and control of switching converters and digital control techniques.

Andrew J. Forsyth (M'98–SM'07) received the B.Sc.(Eng.) degree from Imperial College, London, U.K., in 1981 and the Ph.D. degree from the University of Cambridge, Cambridge, U.K., in 1987.

He was a Design Engineer with GEC Electrical Projects, Ltd., from 1981 to 1983, a Lecturer with the University of Bath from 1986 to 1990, and a Lecturer/Senior Lecturer with Birmingham University from 1991 to 2004. Since 2004, he has been a Professor of power electronics with the School of Electrical and Electronic Engineering, The University of Manchester, Manchester, U.K. His research interests include highfrequency converters, high-power-factor rectifiers, modeling and control of autonomous power systems, and aerospace and electric-vehicle applications.